

Canard cascading in networks with adaptive mean-field coupling

J. Balzer,¹ R. Berner,² K. Lüdge,³ S. Wiczorek,⁴ J. Kurths,^{2,5} and S. Yanchuk^{4,5}

¹*Institut für Theoretische Physik, Technische Universität Berlin, Hardenbergstraße 36, 10623 Berlin, Germany*

²*Department of Physics, Humboldt-Universität zu Berlin, Newtonstr. 15, Berlin, 12489, Germany*

³*Technische Universität Ilmenau, Institut für Physik, Weimarer Straße 25, 98693 Ilmenau, Germany*

⁴*School of Mathematical Sciences, University College Cork, Ireland*

⁵*Potsdam Institute for Climate Impact Research (PIK), Potsdam, Germany*

(Dated: July 31, 2024)

Canard cascading (CC) is observed in dynamical networks with global adaptive coupling. It is a fast-slow phenomenon characterized by a recurrent sequence of fast transitions between distinct and slowly evolving quasi-stationary states. In this letter, we uncover the dynamical mechanisms behind CC, using an illustrative example of globally and adaptively coupled semiconductor lasers, where CC represents sequential switching on and off the lasers. Firstly, we show that CC is a robust and truly adaptive network effect that is scalable with network size and does not occur without adaptation. Secondly, we uncover multiple saddle slow manifolds (unstable quasi-stationary states) linked by heteroclinic orbits (fast transitions) in the phase space of the system. This allows us to identify CC with a novel *heteroclinic canard orbit* that organises different unstable quasi-stationary states into an intricate fast-slow limit cycle. Although individual quasi-stationary states are unstable (saddles), the CC cycle as a whole is attractive and robust to parameter changes.

Dynamical networks with *dynamic nodes* and *static links* are famously universal mathematical models used to describe challenging real-world applications, such as coupled optoelectronic devices, neural networks or power grids [1–8]. In addition to the complex network structure, their nodes are often fast-slow, meaning that they evolve on multiple time scales [9, 10]. Typical examples are coupled semiconductor lasers, where the photon lifetime is much shorter than the carrier lifetime [11, 12], or coupled neurons, where the voltage changes faster than the gating variables [13].

Adaptive dynamical networks (ADNs) with *dynamic nodes* and *dynamic links* are even more advanced mathematical models, where the links between the nodes evolve over time depending on the states of the nodes [14–16]. ADNs capture the interaction between the network function (changing states of the nodes) and network structure (changing strength and arrangement of the links). ADNs are essential for different areas of science, for example, neural plasticity [4], power grid dynamics [17], or decision-making [18], to name a few. Furthermore, they exhibit rich and diverse dynamical behaviors, such as frequency clusters [19], recurrent synchronization [20], different phase transitions [21], explosive synchronization [22, 23]. However, analysis of ADNs is more demanding and often requires new approaches [15].

In this letter, we describe a phenomenon of *canard cascading* (CC) that emerges from an interplay between bistable dynamics of the network nodes and slowly evolving global coupling between the nodes. CC manifests itself as a recurrent sequence of fast transitions between distinct quasi-stationary states. To the best of our knowledge, a first numerical and experimental report on a variant of this phenomenon was given in [24], in the context of the resonance between the dispersion of the network nodes

and the noise strength. Here, we show that CC is a genuine ADN phenomenon that does not occur when the coupling is static. We also show that CC is scalable: the number of quasi-stationary states in the sequence increases proportionally to the network size. Crucially, we uncover the dynamical mechanism underlying CC: a novel heteroclinic canard orbit that organises different unstable quasi-stationary states into an intricate fast-slow limit cycle that is stable and robust to changes in the system parameters.

The general theoretical framework for CC has the form

$$\begin{aligned} du_i/dt &= g(u_i, \omega, X), \\ d\omega/dt &= -\varepsilon[\omega + f(X)], \end{aligned} \quad (1)$$

where $u_i(t)$ is the state of node $i = 1, \dots, N$, $X(t) = N^{-1} \sum_{i=1}^N u_i(t)$ is the mean-field, and $\omega(t)$ is the adaptive coupling variable. The nodes $u_i(t)$ are globally coupled via the direct mean-field $X(t)$ and the adaptive variable $\omega(t)$; see Fig. 1. The small parameter $\varepsilon \ll 1$ quantifies the ratio of the timescales of the slowly-evolving adaptive coupling $\omega(t)$ and fast-changing nodes $u_i(t)$.

To demonstrate and analyse CC in a real-life application, we consider a coupled laser model as in [24]. Recently, there has been much interest in networks of adaptively coupled optoelectronic devices, owing to their potential for neuromorphic computing [25–37]. Therefore, comprehending the dynamics of such systems, and identifying novel dynamical phenomena, is of importance to future machine learning solutions. Our specific model is the network of N coupled semiconductor lasers [38, 39]

$$\begin{aligned} dx_i/dt &= x_i(y_i - 1), \\ dy_i/dt &= \gamma[\delta_i - y_i + k(\omega + f(X)) - x_i y_i], \\ d\omega/dt &= -\varepsilon[\omega + f(X)], \end{aligned} \quad (2)$$

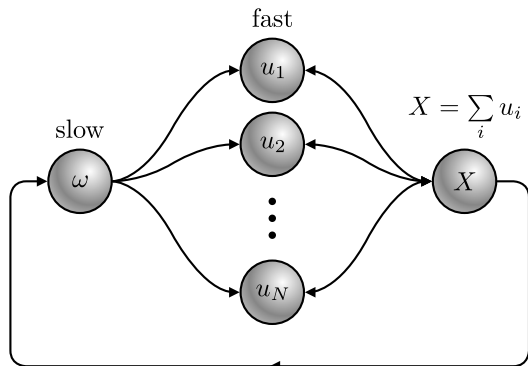


FIG. 1. Adaptive dynamical network with global coupling (1). The nodes u_i are globally coupled via two components: the direct mean-field component $X(t)$ and the slowly-adapting component $\omega(t)$.

where $x_i(t)$ is the light intensity and $y_i(t)$ is the normalized carrier (electron-hole pair) density in laser i . The variable $\omega(t)$ is the feedback electric current that plays the role of global nonlinear adaptive coupling. Its evolution is governed by the signal from the nonlinear amplifier $f(X) = A \ln(1 + \alpha X)$ that receives the mean light intensity $X(t) = N^{-1} \sum_i x_i(t)$, where A and α are two positive feedback parameters. Additional parameters include electric pump currents δ_i and the photodetector responsivity k . Our focus will be on a network of non-identical lasers with different δ_i .

CC in the adaptive laser network manifests itself as a sequence of fast ‘jumps’ in the mean light intensity X (double arrows), each followed by damped oscillations towards a ‘plateau’ of slowly changing feedback current ω with little variation in X (single arrows) in Fig. 2(a)-(b). We will show that these slow plateaus correspond to slow motion along an unstable quasi-stationary state (saddle slow manifold). Such unusual solutions are known in the literature as *canards* [40–48]. Hence the name *canard cascading* (CC). The classical examples of low-dimensional fast-slow limit cycles have one canard segment and are not robust [49]. CC is different in that it consists of *multiple canard segments* and is *robust*. For physically meaningful initial conditions and for a wide parameter range, the system converges to the *CC limit cycle*. While a robust non-classical slow-fast cycle with one canard segment has been identified in [10], CC appears to be the first example with multiple canard segments.

Most importantly, CC is a genuine adaptive network phenomenon: it scales with the network size N and disappears in the absence of adaptation. When we set $\varepsilon = 0$ in (2), treat ω as another parameter, a quasi-static sweep in ω uncovers classical hysteresis in Fig. 2(c). One might expect that when ε is small but non-zero, the adaptive network will closely trace out this hysteresis. However, that is not what happens. Instead, an intricate CC emerges during the transition from the lower to the upper part

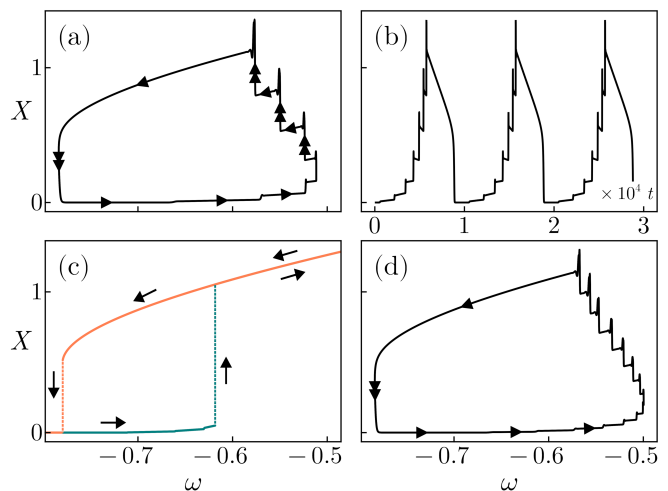


FIG. 2. Simulated CC dynamics of system (2) with $N = 7$ (a-b) and $N = 15$ (d) coupled lasers. (a,d) Projection of the solution onto the (ω, X) -plane. (b) Time series of the mean-field $X(t)$. (c) The non-adaptive case, where ω is a parameter, and parameter scans are performed. The non-adaptive case features a standard hysteresis and no CC. Parameter values: $\gamma = 4 \cdot 10^{-2}$, $\varepsilon = 10^{-4}$, $\delta_i, i = 1, \dots, N$ are chosen equidistantly in the interval $[1.2, 1.505]$, $k = 0.7$, $A = k^{-1}$, and $\alpha = 2$.

of the hysteresis. For $N = 7$ in Fig. 2(a)-(b), this CC consists of seven jumps in X and seven slow plateaus. Numerical results for different N confirm that the phenomenon scales with N and appears to be universal, see e.g. the case $N = 15$.

We will now describe the mechanism behind CC and show that the fast jumps occur along special heteroclinic orbits connecting different unstable quasi-stationary states. We begin by identifying quasi-stationary states and their stability. In the terminology of geometric singular perturbation theory [50–53], we identify branches of the critical manifold for system (2).

To obtain all quasi-stationary states, stable and unstable, we perform the adiabatic elimination of the fast laser field x_i and carrier density y_i by setting $\dot{x}_i = 0$ and $\dot{y}_i = 0$ in system (2). This gives the following solutions: the i -th laser is either ‘off’ $(x_i, y_i) = (0, \delta_i + k[\omega + f(X)])$ or ‘on’ $(x_i, y_i) = (\delta_i - 1 + k[\omega + f(X)], 1)$ for all i . In other words, there is one branch of the critical manifold for every combination where some lasers are ‘on’ and the other lasers are ‘off’. If the set of all N_+ lasers that are ‘on’ is denoted with I_+ , then the corresponding branch of the critical manifold is given by

$$(x_i, y_i) = \begin{cases} (0, \delta_i + k[\omega + f(X)]) & \text{for } i \notin I_+, \\ (\delta_i - 1 + k[\omega + f(X)], 1) & \text{for } i \in I_+, \end{cases} \quad (3)$$

where the mean-field satisfies the self-consistency equa-

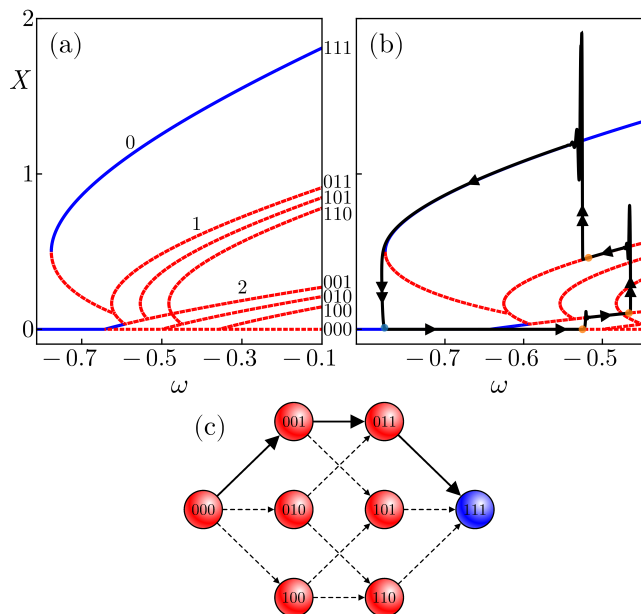


FIG. 3. (a) Critical manifold branches of system (2) of three coupled lasers. Projection onto the (ω, X) -plane. Stable parts are shown as solid blue lines and unstable parts as dashed red lines. The labels on the right vertical axis show which lasers are "on" (1) or "off" (0). The numbers on the branches indicate the number of their unstable dimensions. (b) A zoom of part of (a) with CC solution shown by the solid black line. Theoretical predictions for the jump points are shown as orange dots. (c) Schematic representation of the network of heteroclinic connections with solid lines showing the connections along the CC solution. Parameters: $\delta = (1.25, 1.35, 1.45)$, $k = 0.7$, $A = k^{-1}$, and $\alpha = 2$.

tion

$$X = \frac{N_+}{N} [\bar{\delta} - 1 + k(\omega + f(X))], \quad (4)$$

with $\bar{\delta} = N_+^{-1} \sum_{i \in I_+} \delta_i$ being the average pump of all lasers that are "on". Since there are 2^N different combinations, there are also 2^N different branches of the critical manifold leading to 2^N possible quasi-stationary states.

For $N = 3$ lasers, Fig. 3(a) shows all $2^N = 8$ branches of the critical manifold, in projection onto the (X, ω) plane. Each branch is a one-dimensional curve in the $2N + 1 = 7$ -dimensional phase space of system (2). The stable branches are plotted in blue, while (unstable) saddle branches are plotted in red; see [54] for the stability analysis. We also introduce the notations $B_{000}, B_{001}, \dots, B_{111}$ for the branches of the critical manifold, where "1" stands for laser "on" and "0" for laser "off", with the lasers ordered in ascending order of their pump currents δ_i .

The critical manifold has the following properties. First, most of the branches are unstable and saddle-type, meaning that they have both repelling and attracting directions. The exceptions are B_{111} , a part of B_{000} , and a

small part of B_{001} , which are stable. Two different stable branches co-exist for some interval of ω in Fig. 2(c), giving rise to bistability and the classical hysteresis upon quasi-static change in ω . Second, the branches corresponding to the same number N_+ of active lasers are closely grouped. Their separation is proportional to the mismatch in the pump currents δ_i .

The CC limit cycle together with all branches of the critical manifold is shown in Fig. 3(b). The cycle follows certain branches for significant periods of time, including those identified as unstable (saddles). In addition, fast transitions to unstable branches are observed. This unusual behaviour raises the following questions. (q1) Why does the system jump towards unstable branches? (q2) What is the physical interpretation of such jumps? (q3) How does the system choose a particular unstable branch from each family to jump to? (q4) Why does the system follow these unstable branches for a significant amount of time? (q5) Can we estimate this time?

Owing to the letter format of this publication, we now give conceptual answers to these questions, and move the supporting technical details to [54].

(q1) We begin by answering question (q1). The jumps between two unstable (saddle) branches of the critical manifold are enabled by robust paths between these branches in the phase space, also known as *robust heteroclinic connecting orbits* [55, 56]; see the schematic diagram in Fig. 3(c). The main reasons for the appearance of these heteroclinic orbits are twofold:

Firstly, we observe that branches with more active lasers branch off branches with less active lasers, e.g. B_{001}, B_{010} and B_{001} branch off B_{000} . The branching rule is that if a branch B_{mnl} branches off B_{ijk} , then $(m + n + l) - (i + j + k) = 1$ [57]. Such a branching rule leads to the connectivity graph G in Fig. 3(c) for sufficiently large ω . For smaller ω , a subgraph of G is realised. Each branching point corresponds to a transcritical bifurcation of equilibria in the "layer system" parametrised by ω (i.e. system (2) with $\varepsilon = 0$). Therefore, for a fixed ω , each arrow in the graph corresponds to a heteroclinic orbit in the layer system connecting two branches.

Secondly, the heteroclinic connections are robust. This robustness is due to the existence of invariant subspaces. For example, for a given ω , the heteroclinic orbit $B_{000} \rightarrow B_{001}$ lies in the 4-dimensional invariant subspace $x_1 = x_2 = 0$. Within the invariant subspace, it connects a saddle with one unstable direction to an attractor. The same is true for every other heteroclinic connection in Fig. 3(c). In other words, these heteroclinic connections are robust for the flow restricted to their corresponding invariant subspace, similar to [55, 58–60]. Since changes in ω preserve invariant subspaces, these heteroclinic orbits are robust to changes in ω . This is why they manifest in the full system with changing ω (i.e. system (2) with $\varepsilon > 0$). More generally, even in the absence of invariant

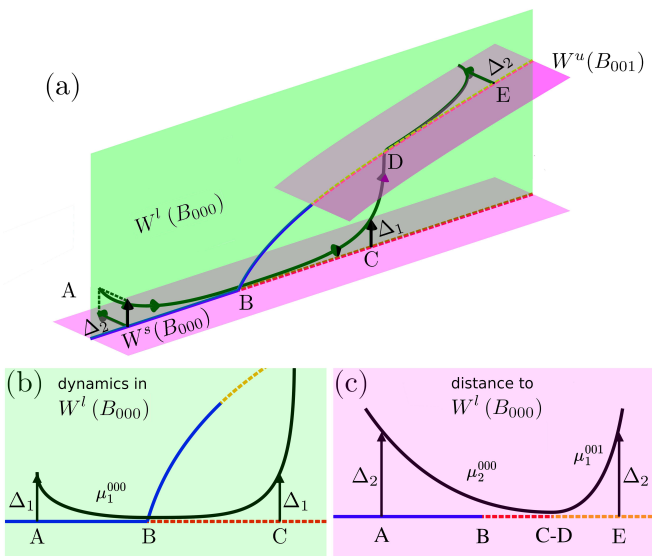


FIG. 4. Schematic description of CC jumps for the branches B_{000} and B_{001} for the case of three lasers; see details in the text.

subspaces, these heteroclinic connections would be robust because they are transverse intersections of unstable and stable invariant manifolds of two saddle branches, as is also the case in the Olsen model [56], see more details in [54].

(q2) We have shown that there is a correspondence between the directed graph G in Fig. 3(c) and the heteroclinic connections among the branches of the critical manifold. These connections have a clear physical meaning: each connection $B_I \rightarrow B_J$ with $I = a_1 \dots a_i \dots a_N$ and $J = a_1 \dots a_i + 1 \dots a_N$ corresponds to a fast increase of the laser i intensity from 0 to the value $\delta_i - 1 + k[\omega + f(X)]$.

(q3) According to the obtained graph of heteroclinic connections, the system can potentially evolve along any directed path in this graph during the time evolution starting from the off-state. However, CC is realised along a specific path in the graph, corresponding to the sequential activation of the lasers with the highest pump current δ_i ; see the highlighted path in Fig. 3(c). The theoretical reason for this path selection is that the highlighted path corresponds to the most unstable direction that the system chooses in the case of several "exit possibilities". As a consequence, the CC phenomenon does not exist for identical coupled lasers, when all N connections from $B_{0\dots 0}$ to the branches with a single laser "on" are equally unstable, and there is no preferred direction that would define a cascading path. As a result, the symmetric system jumps directly to the stable branch $B_{1\dots 1}$, avoiding the heteroclinic connections even though they are present.

(q4) Figure 4 illustrates the geometric mechanism of CC as the interplay between the branches B_I , their stable

and unstable manifolds, and the heteroclinic connections between them. The figure shows the "leading manifold" $W^l(B_{000})$ of the branch B_{000} , which is defined by the most unstable (least stable) direction of B_{000} [61]. The manifold $W^l(B_{000})$ contains B_{001} . Since the CC solution is repelled from B_{000} along $W^l(B_{000})$, it is attracted to the branch B_{001} , even though B_{001} is unstable. Further, the leading unstable manifold $W^u(B_{001})$ of B_{001} is shown in magenta in Fig. 4. The time the system spends near B_{001} depends on the initial distance of the system to $W^l(B_{000})$ and the rate at which the instability develops along B_{001} .

(q5) Now we explain what determines the duration of the slow motions along the unstable branches, see Fig. 4. The part AB of the trajectory shows the approaching to B_{000} and a drift along the stable part of this branch. The duration and rate of convergence to B_{000} determines how long the trajectory remains close to B_{000} during the BC phase. The ABC phase is a standard delayed exchange stability [62, 63] with the additional simplification that the state B_{000} does not depend on ω . Thus, the jumping condition at $\omega = \omega_C$ is given by

$$\int_{\omega_A}^{\omega_C} \frac{\mu_1^{000}(\omega)}{\omega + f(X_{000})} d\omega = 0, \quad (5)$$

where μ_1^{000} is the leading unstable eigenvalue at B_{000} , $X_{000} = 0$ is the corresponding mean-field. The theoretically predicted jump point at $\omega = \omega_C$ for the case $N = 3$ (orange dot in Fig. 3(b)) agrees with the actual jump of the black trajectory.

We will now explain the mechanism behind the other jump points using the slow motion at the branch B_{001} , see Fig. 4. The distance $\Delta_2(t)$ from the leading manifold $W^l(B_{000})$ (green in the figure) decreases during the phase ABC along the direction that is transverse to $W^l(B_{000})$ (determined by the second largest eigenvalue μ_2^{000}), and the repulsion during the phase DE along the most unstable direction of B_{001} (determined by the largest eigenvalue μ_1^{001}). As a result, the conditions for the second jump point is

$$\int_{\omega_A}^{\omega_C} \frac{\mu_2^{000}(\omega)}{\omega + f(X_{000})} d\omega + \int_{\omega_C}^{\omega_E} \frac{\mu_1^{001}(\omega)}{\omega + f(X_{001})} d\omega = 0. \quad (6)$$

Here we used $\omega_C \approx \omega_D$ as the jump occurs on the fast timescale. Supplemental material [54] provides more detail.

In summary, we have presented the explanation for the emergence and the main ingredients of canard cascading (CC). These ingredients are (i) multiple branches of low-dimensional critical manifolds. The number of such branches grows extensively with the size of the network. (ii) Robust heteroclinic connections, which allow for fast transitions between unstable branches. (iii) Delayed exchange of stability on the critical manifold allows the appearance of canard solutions following the unstable parts

of the branches.(iv) Finally, the heterogeneity of the individual elements is necessary for the switching behaviour.

While our study focuses on coupled semiconductor lasers and is directly related to an experimentally observed effect, CC is expected in a variety of other setups, such as neural or ecological systems. From a modelling point of view, the important elements seem to be very general: global coupling to an active low-pass filter [64] and heterogeneity of interacting elements.

SY, RB, and JK acknowledge funding by the "Deutsche Forschungsgemeinschaft" (DFG), Project 411803875.

-
- [1] A. Pikovsky, M. Rosenblum, and J. Kurths, *Synchronization. A Universal Concept in Nonlinear Sciences* (Cambridge University Press, 2001).
- [2] S. Boccaletti, V. Latora, Y. Moreno, M. Chavez, and D.-U. Hwang, Complex networks: Structure and dynamics, *Phys. Rep.* **424**, 175 (2006).
- [3] M. C. Soriano, J. García-Ojalvo, C. R. Mirasso, and I. Fischer, Complex photonics: Dynamics and applications of delay-coupled semiconductor lasers, *Reviews of Modern Physics* **85**, 421 (2013).
- [4] W. Gerstner, W. M. Kistler, R. Naud, and L. Paninski, *Neuronal Dynamics* (Cambridge University Press, Cambridge, 2014).
- [5] F. Hellmann, P. Schultz, P. Jaros, R. Levchenko, T. Kapitaniak, J. Kurths, and Y. Maistrenko, Network-induced multistability through lossy coupling and exotic solitary states, *Nature Communications* **11**, 592 (2020).
- [6] B. Schäfer, D. Witthaut, M. Timme, and V. Latora, Dynamically induced cascading failures in power grids, *Nature Communications* **9**, 1 (2018).
- [7] M. Newman, *Networks* (Oxford University Press, 2018).
- [8] V. Nicosia, P. S. Skardal, A. Arenas, and V. Latora, Collective Phenomena Emerging from the Interactions between Dynamical Processes in Multiplex Networks, *Physical Review Letters* **118**, 138302 (2017).
- [9] M. Desroches, J. Guckenheimer, B. Krauskopf, C. Kuehn, H. M. Osinga, and M. Wechselberger, Mixed-Mode Oscillations with Multiple Time Scales, *SIAM Review* **54**, 211 (2012), publisher: Society for Industrial and Applied Mathematics.
- [10] C. Kuehn, *Multiple Time Scale Dynamics*, Vol. 191 (Springer-Verlag GmbH, 2015) publication Title: Springer ISSN: 0066-5452.
- [11] T. Erneux and D. Lenstra, Synchronization of Mutually Delay-Coupled Quantum Cascade Lasers with Distinct Pump Strengths, *Photonics* **6**, 125 (2019), publisher: MDPI AG.
- [12] A. Roos, S. Meinecke, and K. Lüdge, Stabilizing nanolasers via polarization lifetime tuning, *Scientific Reports* **11**, 18558 (2021).
- [13] E. M. Izhikevich, Neural excitability, spiking and bursting, *International Journal of Bifurcation and Chaos* **10**, 1171 (2000).
- [14] T. Gross and B. Blasius, Adaptive coevolutionary networks: a review, *Journal of The Royal Society Interface* **5**, 259 (2008).
- [15] R. Berner, T. Gross, C. Kuehn, J. Kurths, and S. Yanchuk, Adaptive dynamical networks, *Physics Reports* **1031**, 1 (2023).
- [16] J. Sawicki, R. Berner, S. A. M. Loos, M. Anvari, R. Bader, W. Barfuss, N. Botta, N. Brede, I. Franović, D. J. Gauthier, S. Goldt, A. Hajizadeh, P. Hövel, O. Karin, P. Lorenz-Spreen, C. Miehl, J. Mölter, S. Olmi, E. Schöll, A. Seif, P. A. Tass, G. Volpe, S. Yanchuk, and J. Kurths, Perspectives on adaptive dynamical systems, *Chaos: An Interdisciplinary Journal of Nonlinear Science* **33**, 071501 (2023).
- [17] R. Berner, S. Yanchuk, and E. Schöll, What adaptive neuronal networks teach us about power grids, *Physical Review E* **103**, 042315 (2021), publisher: American Physical Society.
- [18] L. Chen, C. Huepe, and T. Gross, Adaptive network models of collective decision making in swarming systems, *Phys. Rev. E* **94**, 022415 (2016).
- [19] R. Berner, E. Schöll, and S. Yanchuk, Multiclusters in networks of adaptively coupled phase oscillators, *SIAM Journal on Applied Dynamical Systems* **18**, 2227 (2019).
- [20] M. Thiele, R. Berner, P. A. Tass, E. Schöll, and S. Yanchuk, Asymmetric adaptivity induces recurrent synchronization in complex networks, *Chaos: An Interdisciplinary Journal of Nonlinear Science* **33**, 023123 (2023), publisher: AIP Publishing LLC/AIP Publishing.
- [21] J. Fialkowski, S. Yanchuk, I. M. Sokolov, E. Schöll, G. A. Gottwald, and R. Berner, Heterogeneous Nucleation in Finite-Size Adaptive Dynamical Networks, *Physical Review Letters* **130**, 067402 (2023), publisher: American Physical Society.
- [22] C. Zhou and J. Kurths, Dynamical weights and enhanced synchronization in adaptive complex networks, *Physical review letters* **96**, 164102 (2006), publisher: APS.
- [23] V. Avalos-Gaytán, J. A. Almendral, I. Leyva, F. Battiston, V. Nicosia, V. Latora, and S. Boccaletti, Emergent explosive synchronization in adaptive complex networks, *Physical Review E* **97**, 042301 (2018).
- [24] O. D’Huys, R. Veltz, A. Dolcemascio, F. Marino, and S. Barland, Canard resonance: on noise-induced ordering of trajectories in heterogeneous networks of slow-fast systems, *Journal of Physics: Photonics* **3**, 024010 (2021).
- [25] L. Appeltant, M. C. Soriano, G. V. D. Sande, J. Danckaert, S. Massar, J. Dambre, B. Schrauwen, C. R. Mirasso, and I. Fischer, Information processing using a single dynamical node as complex system, *Nature Communications* **2**, 1 (2011).
- [26] B. Romeira, R. Avó, J. M. L. Figueiredo, S. Barland, and J. Javaloyes, Regenerative memory in time-delayed neuromorphic photonic resonators, *Scientific Reports* **6**, 19510 (2016).
- [27] L. Larger, A. Baylón-Fuentes, R. Martinenghi, V. S. Udaltsov, Y. K. Chembo, and M. Jacquot, High-Speed Photonic Reservoir Computing Using a Time-Delay-Based Architecture: Million Words per Second Classification, *Physical Review X* **7**, 011015 (2017).
- [28] D. Brunner, B. Penkovsky, B. A. Marquez, M. Jacquot, I. Fischer, and L. Larger, Tutorial: Photonic neural networks in delay systems, *Journal of Applied Physics* **124**, 152004 (2018), arXiv: 2111.03332.
- [29] A. Argyris, J. Cantero, M. Galletero, E. Pereda, C. R. Mirasso, I. Fischer, and M. C. Soriano, Comparison of Photonic Reservoir Computing Systems for Fiber Transmission Equalization,

- IEEE Journal of Selected Topics in Quantum Electronics **26**, 1 (2020), publisher: IEEE.
- [30] J. Robertson, M. Hejda, J. Bueno, and A. Hurtado, Ultrafast optical integration and pattern classification for neuromorphic photonics based on spiking VCSEL neurons, *Scientific Reports* **10**, 6098 (2020).
- [31] F. Stelzer, A. Röhm, R. Vicente, I. Fischer, and S. Yanchuk, Deep neural networks using a single neuron: folded-in-time architecture using feedback-modulated delay loops, *Nature Communications* **12**, 5164 (2021), arXiv: 2011.10115 Publisher: Nature Publishing Group.
- [32] S. Apostel, N. D. Haynes, E. Schöll, O. D’Huys, and D. J. Gauthier, Reservoir Computing Using Autonomous Boolean Networks Realized on Field-Programmable Gate Arrays, in *Reservoir Computing: Theory, Physical Implementations, and Applications*, edited by K. Nakajima and I. Fischer (Springer, Singapore, 2021) pp. 239–271.
- [33] C. Huang, V. J. Sorger, M. Miscuglio, M. Al-Qadasi, A. Mukherjee, L. Lampe, M. Nichols, A. N. Tait, T. Ferreira De Lima, B. A. Marquez, J. Wang, L. Chrostowski, M. P. Fok, D. Brunner, S. Fan, S. Shekhar, P. R. Prucnal, and B. J. Shastri, Prospects and applications of photonic neural networks, *Advances in Physics: X* **7**, 1981155 (2022).
- [34] A. Lupo, E. Picco, M. Zajnulina, and S. Massar, Deep photonic reservoir computer based on frequency multiplexing with fully analog connection between layers, *Optica* **10**, 1478 (2023).
- [35] S. Biasi, G. Donati, A. Lugnan, M. Mancinelli, E. Staffoli, and L. Pavesi, Photonic Neural Networks Based on Integrated Silicon Microresonators, *Intelligent Computing* **3**, 0067 (2024).
- [36] J. Henaff, M. Ansquer, M. C. Soriano, R. Zambini, N. Treps, and V. Parigi, Optical phase encoding in a pulsed approach to reservoir computing, *Optics Letters* **49**, 2097 (2024).
- [37] S. Deligiannidis, K. R. H. Bottrill, K. Sozos, C. Mesaritakis, P. Petropoulos, and A. Bogris, Multichannel Nonlinear Equalization in Coherent WDM Systems Based on Bi-Directional Recurrent Neural Networks, *Journal of Lightwave Technology* **42**, 541 (2024).
- [38] A. Dolcemascolo, A. Miazek, R. Veltz, F. Marino, and S. Barland, Effective low-dimensional dynamics of a mean-field coupled network of slow-fast spiking lasers, *Physical Review E* **101**, 052208 (2020).
- [39] K. Al-Naimee, F. Marino, M. Ciszak, R. Meucci, and F. T. Arecchi, Chaotic spiking and incomplete homoclinic scenarios in semiconductor lasers with optoelectronic feedback, *New Journal of Physics* **11**, 073022 (2009).
- [40] E. Benoît, J. L. Callot, F. Diener, and M. Diener, Chasse au canard (première partie), *Collectanea Mathematica* , 37 (1981).
- [41] K. Bold, C. Edwards, J. Guckenheimer, S. Guharay, K. Hoffman, J. Hubbard, R. Oliva, and W. Weckesser, The Forced van der Pol Equation II: Canards in the Reduced System, *SIAM Journal on Applied Dynamical Systems* **2**, 570 (2003).
- [42] W. Eckhaus, Relaxation oscillations including a standard chase on French ducks, in *Asymptotic Analysis II* —, edited by F. Verhulst (Springer Berlin Heidelberg, Berlin, Heidelberg, 1983) pp. 449–497.
- [43] M. Krupa and P. Szmolyan, Relaxation Oscillation and Canard Explosion, *Journal of Differential Equations* **174**, 312 (2001), publisher: Academic Press.
- [44] B. Peng, V. Gaspar, and K. Showalter, False bifurcations in chemical systems: canards, *Philosophical Transactions of the Royal Society of London. Series A* , publisher: The Royal Society London.
- [45] P. Szmolyan and M. Wechselberger, Canards in R^3 , *Journal of Differential Equations* **177**, 419 (2001), publisher: Academic Press.
- [46] M. Wechselberger, Existence and Bifurcation of Canards in R^3 in the Case of a Folded Node, *SIAM Journal on Applied Dynamical Systems* **4**, 101 (2005).
- [47] M. Wechselberger, J. Mitry, and J. Rinzel, Canard Theory and Excitability, in *Lecture Notes in Mathematics*, Vol. 2102 (2013) pp. 89–132, ISSN: 00758434.
- [48] P. E. Sullivan, K. Mulchrone, and S. Wiczorek, Rate-induced tipping to metastable zombie fires, *Proceedings of the Royal Society A* **479**, 20220647 (2023).
- [49] M. Wechselberger, Canards, *Scholarpedia* **2**, 1356 (2007).
- [50] N. Fenichel, Geometric singular perturbation theory for ordinary differential equations, *Journal of Differential Equations* **31**, 53 (1979), publisher: Academic Press.
- [51] H. Jardon-Kojakhmetov and C. Kuehn, A survey on the blow-up method for fast-slow systems, arXiv: 1901.01402 (2019).
- [52] C. K. R. T. Jones, Geometric singular perturbation theory BT - Dynamical Systems: Lectures Given at the 2nd Session of the Centro Internazionale Matematico Estivo (C.I.M.E.) held in Montecatini Terme, Italy, June 13–22, 1994 (Springer Berlin Heidelberg, Berlin, Heidelberg, 1995) pp. 44–118.
- [53] M. Wechselberger, *Geometric Singular Perturbation Theory Beyond* Frontiers in Applied Dynamical Systems: Reviews and Tutorials, Vol. 6 (Springer International Publishing, Cham, 2020).
- [54] See Supplemental Material at URL-will-be-inserted-by-publisher for the stability analysis of the critical manifold, description of the heteroclinic connections between the slow manifolds and their genericity, and calculation of the jump points.
- [55] M. Krupa, Robust heteroclinic cycles, *Journal of Nonlinear Science* **7**, 129 (1997).
- [56] E. Musoke, B. Krauskopf, and H. M. Osinga, A Surface of Heteroclinic Connections Between Two Saddle Slow Manifolds in the Olsen Model, *International Journal of Bifurcation and Chaos* **10.1142/S0218127420300487** (2020).
- [57] This rule can be violated in the presence of a symmetry, e.g., when the lasers are identical [54].
- [58] P. Ashwin and J. Borresen, Discrete computation using a perturbed heteroclinic network, *Physics Letters A* **347**, 208 (2005).
- [59] P. Ashwin, O. Burylko, and Yu. Maistrenko, Bifurcation to heteroclinic cycles and sensitivity in three and four coupled phase oscillators, *Physica D* **237**, 454 (2008).
- [60] P. Ashwin, G. Orosz, and J. Borresen, Heteroclinic Switching in Coupled Oscillator Networks: Dynamics on Odd Graphs, in *Understanding Complex Systems*, Vol. 2010 (Springer Verlag, 2010) pp. 31–50.
- [61] More precisely, a perturbation of the family of leading stable, centre and leading unstable manifolds of the corresponding equilibria of the layer system parameterized by ω .

- [62] S. M. Baer, T. Erneux, and J. Rinzel, The Slow Passage through a Hopf Bifurcation: Delay, Memory Effects, and Resonance, *SIAM Journal on Applied Mathematics* **49**, 55 (1989).
- [63] J. Su, The Phenomenon of Delayed Bifurcation and its Analyses, in *Multiple-Time-Scale Dynamical Systems*, edited by C. K. R. T. Jones and A. I. Khibnik (Springer, New York, NY, 2001) pp. 203–214.
- [64] M. Ciszak, S. Olmi, G. Innocenti, A. Torcini, and F. Marino, Collective canard explosions of globally-coupled rotators with adaptive coupling, *Chaos, Solitons & Fractals* **153**, 111592 (2021).

A.I. STABILITY ANALYSIS OF THE CRITICAL MANIFOLD

In the main part of the paper, we have introduced the critical manifold (see Eqs. (3) and (4) in the manuscript), which consists of branches B_I . In this section, we derive the stability conditions for B_I . For this, we linearize the fast system along these branches and study the linear stability of the linearizations obtained.

Let us introduce the following notations for the right-hand sides of the fast system

$$\begin{aligned} h_{i,1}(x_i, y_i) &:= x_i(y_i - 1), \\ h_{i,2}(x_i, y_i, \omega) &:= \gamma[\delta_i - y_i + k(\omega + f(X)) - x_i y_i], \end{aligned}$$

where $X = \frac{1}{N} \sum_i x_i$ and $f(X) = A \ln(1 + \frac{\alpha}{N} \sum_i x_i)$. Then the Jacobian of the fast system is

$$D_{\mathbf{x}, \mathbf{y}} \mathbf{h} = \begin{bmatrix} \frac{\partial h_{1,1}}{\partial x_1} & \frac{\partial h_{1,1}}{\partial y_1} & \dots & \frac{\partial h_{1,1}}{\partial x_N} & \frac{\partial h_{1,1}}{\partial y_N} \\ \frac{\partial h_{1,2}}{\partial x_1} & \frac{\partial h_{1,2}}{\partial y_1} & \dots & \frac{\partial h_{1,2}}{\partial x_N} & \frac{\partial h_{1,2}}{\partial y_N} \\ \vdots & \vdots & \ddots & \vdots & \vdots \\ \frac{\partial h_{N,1}}{\partial x_1} & \frac{\partial h_{N,1}}{\partial y_1} & \dots & \frac{\partial h_{N,1}}{\partial x_N} & \frac{\partial h_{N,1}}{\partial y_N} \\ \frac{\partial h_{N,2}}{\partial x_1} & \frac{\partial h_{N,2}}{\partial y_1} & \dots & \frac{\partial h_{N,2}}{\partial x_N} & \frac{\partial h_{N,2}}{\partial y_N} \end{bmatrix}. \quad (7)$$

The Jacobian contains the following 2×2 -blocks

$$\begin{pmatrix} \frac{\partial h_{i,1}}{\partial x_i} & \frac{\partial h_{i,1}}{\partial y_i} \\ \frac{\partial h_{i,2}}{\partial x_i} & \frac{\partial h_{i,2}}{\partial y_i} \end{pmatrix} = \begin{pmatrix} y_i - 1 & x_i \\ \gamma \left[\frac{kA\alpha}{N(1+\alpha X)} - y_i \right] & -\gamma(x_i + 1) \end{pmatrix} \quad (8)$$

along the diagonal, and all the remaining 2×2 blocks have the form

$$\begin{pmatrix} \frac{\partial h_{i,1}}{\partial x_j} & \frac{\partial h_{i,1}}{\partial y_j} \\ \frac{\partial h_{i,2}}{\partial x_j} & \frac{\partial h_{i,2}}{\partial y_j} \end{pmatrix} = \begin{pmatrix} 0 & 0 \\ \gamma \frac{kA\alpha}{N(1+\alpha X)} & 0 \end{pmatrix}, \quad i \neq j. \quad (9)$$

Now consider the branch $B_I = B_{a_1 \dots a_N}$, where $a_i = 1$ if the laser i is on and $a_i = 0$ if the laser i is off. Then $N_+ = \sum_i a_i$ is the number of lasers switched on for the solution on this branch. The corresponding mean field X_I satisfies

$$X_I = \frac{1}{N} \sum_i x_i = \frac{1}{N} \sum_{i \in I_+} (\delta_i - 1 + k[\omega + f(X_I)]) = \frac{N_+}{N} [\bar{\delta}_I - 1 + k(\omega + f(X_I))],$$

which leads to the equation (4) from the main part of the manuscript.

Restricting the Jacobian to the branch B_I , we obtain

$$\mathbf{J}_c := \begin{pmatrix} 0 & 0 \\ \gamma \frac{kA\alpha}{N(1+\alpha X_I)} & 0 \end{pmatrix}$$

for the non-diagonal blocks (9). For the diagonal blocks (8), we obtain the following two cases depending on whether the laser i is on or off:

$$\mathbf{J}_{\text{on}, i} := \begin{pmatrix} 0 & \delta_i - 1 + k[\omega + f(X_I)] \\ \gamma \left[\frac{kA\alpha}{N(1+\alpha X_I)} - 1 \right] & -\gamma(\delta_i + k[\omega + f(X_I)]) \end{pmatrix}, \quad \text{if } a_i = 1$$

and

$$\mathbf{J}_{\text{off},i} := \begin{pmatrix} \delta_i + k[\omega + f(X_I)] - 1 & 0 \\ \gamma \left[\frac{kA\alpha}{N(1+\alpha X_I)} - \delta_i - k[\omega + f(X_I)] \right] & -\gamma \end{pmatrix}, \quad \text{if } a_i = 0.$$

Without loss of generality, let us assume that the first N_+ lasers on the branch B_I are on. Then the Jacobian for B_I has the following block structure:

$$J_I := D_{\mathbf{x},\mathbf{y}}\mathbf{h}|_{B_I} = \left[\begin{array}{c|c} \mathbf{ON}_{N_+} & \mathbf{C}_{N_+ \times N_-} \\ \hline \mathbf{C}_{N_- \times N_+} & \mathbf{OFF}_{N_-} \end{array} \right] \in \mathbb{R}^{2N \times 2N}, \quad (10)$$

where

$$\mathbf{C}_{p \times q} = \begin{bmatrix} \mathbf{J}_c & \cdots & \mathbf{J}_c \\ \vdots & \ddots & \vdots \\ \mathbf{J}_c & \cdots & \mathbf{J}_c \end{bmatrix} \in \mathbb{R}^{2p \times 2q}, \quad (11)$$

$$\mathbf{ON}_{N_+} = \begin{bmatrix} \mathbf{J}_{\text{on},1} & \mathbf{J}_c & \cdots & \mathbf{J}_c \\ \mathbf{J}_c & \mathbf{J}_{\text{on},2} & \ddots & \vdots \\ \vdots & \ddots & \ddots & \mathbf{J}_c \\ \mathbf{J}_c & \cdots & \mathbf{J}_c & \mathbf{J}_{\text{on},N_+} \end{bmatrix} \in \mathbb{R}^{2N_+ \times 2N_+}, \quad (12)$$

$$\mathbf{OFF}_{N_-} = \begin{bmatrix} \mathbf{J}_{\text{off},N_++1} & \mathbf{J}_c & \cdots & \mathbf{J}_c \\ \mathbf{J}_c & \mathbf{J}_{\text{off},N_++2} & \ddots & \vdots \\ \vdots & \ddots & \ddots & \mathbf{J}_c \\ \mathbf{J}_c & \cdots & \mathbf{J}_c & \mathbf{J}_{\text{off},N} \end{bmatrix} \in \mathbb{R}^{2N_- \times 2N_-}. \quad (13)$$

A.I.1. Symmetric case

Here we consider the symmetric case, i.e. all lasers are identical with $\delta = \delta_i$ for all i . This case could equivalently be called "homogeneous", but we use "symmetric" throughout for consistency. Then the corresponding blocks $\mathbf{J}_{\text{on},i} = \mathbf{J}_{\text{on}}$ and $\mathbf{J}_{\text{off},i} = \mathbf{J}_{\text{off}}$ become identical, where

$$\mathbf{J}_{\text{on}} = \begin{pmatrix} 0 & \delta - 1 + k[\omega + f(X_I)] \\ \gamma \left[\frac{kA\alpha}{N(1+\alpha X_I)} - 1 \right] & -\gamma(\delta + k[\omega + f(X_I)]) \end{pmatrix}, \quad (14)$$

$$\mathbf{J}_{\text{off}} = \begin{pmatrix} \delta + k[\omega + f(X_I)] - 1 & 0 \\ \gamma \left[\frac{kA\alpha}{N(1+\alpha X_I)} - \delta - k[\omega + f(X_I)] \right] & -\gamma \end{pmatrix}. \quad (15)$$

This enables us to find the eigenvalues analytically. To formulate our results in a more structured way, we formulate the next result as a lemma.

Lemma 1 [Dimension reduction of the eigenvalue problem]. *The eigenvalue problem*

$$\mathbf{J}_I \mathbf{v} = \lambda \mathbf{v} \quad (16)$$

can be reduced in the symmetric case and for $1 \leq N_+ < N$ to the following three eigenvalue problems

$$[\mathbf{J}_{\text{on}} - \mathbf{J}_c] \mathbf{z}_{\text{on}} = \lambda_{\text{on}} \mathbf{z}_{\text{on}}, \quad (17)$$

$$[\mathbf{J}_{\text{off}} - \mathbf{J}_c] \mathbf{z}_{\text{off}} = \lambda_{\text{off}} \mathbf{z}_{\text{off}}, \quad (18)$$

and

$$\begin{bmatrix} [\mathbf{J}_{\text{on}} + (N_+ - 1)\mathbf{J}_c] & N_- \mathbf{J}_c \\ N_+ \mathbf{J}_c & [\mathbf{J}_{\text{off}} + (N_- - 1)\mathbf{J}_c] \end{bmatrix} \begin{pmatrix} \mathbf{a} \\ \mathbf{b} \end{pmatrix} = \lambda \begin{pmatrix} \mathbf{a} \\ \mathbf{b} \end{pmatrix}. \quad (19)$$

More specifically, the following are the eigenvector-eigenvalue pairs of (16)

$$\begin{aligned} & ((\mathbf{v}_k \otimes \mathbf{z}_{\text{on}}), \lambda_{\text{on}}), \quad k = 1, \dots, N_+ - 1, \\ & ((\mathbf{w}_k \otimes \mathbf{z}_{\text{off}}), \lambda_{\text{off}}), \quad k = 1, \dots, N_- - 1 \end{aligned}$$

with

$$\begin{aligned} \mathbf{v}_k &= (\omega_k, \omega_k^2, \dots, \omega_k^{N_+}, 0, \dots, 0)^T, \\ \mathbf{w}_k &= (0, \dots, 0, \mu_k, \mu_k^2, \dots, \mu_k^{N_-})^T \end{aligned}$$

and

$$\omega_k^j = \exp\left(\frac{2\pi i}{N_+} jk\right), \quad \mu_k^j = \exp\left(\frac{2\pi i}{N_-} jk\right),$$

if $(\mathbf{z}_{\text{on}}, \lambda_{\text{on}})$ or $(\mathbf{z}_{\text{off}}, \lambda_{\text{off}})$ are the eigenvector-eigenvalue pairs of (17) or (18).

Likewise,

$$\left(\begin{pmatrix} \mathbf{1}_{N_+} \otimes \mathbf{a} \\ \mathbf{1}_{N_-} \otimes \mathbf{b} \end{pmatrix}, \lambda \right)$$

is the eigenvector-eigenvalue pair of (16) if $((\mathbf{a}, \mathbf{b}), \lambda)$ is the eigenvector-eigenvalue pair of (19). In this way, we reduce the eigenvalues problem (16) to the low-dimensional problems (17), (18), and (19).

Proof. We will prove the reduction to (17) with the family of vectors \mathbf{v}_k . Consider $\mathbf{z}_{\text{on}} \neq \mathbf{0}$ to be the eigenvector of the reduced problem (23) with the eigenvalue λ_{on} . The identity $\mathbf{J}_I(\mathbf{v}_k \otimes \mathbf{z}_{\text{on}}) = \lambda_{\text{on}}(\mathbf{v}_k \otimes \mathbf{z}_{\text{on}})$ follows from the following calculations:

$$\begin{aligned} \mathbf{J}_I(\mathbf{v}_k \otimes \mathbf{z}_{\text{on}}) &= \left[\begin{array}{c|c} \mathbf{ON}_{N_+} & \mathbf{C}_{N_+ \times N_-} \\ \mathbf{C}_{N_- \times N_+} & \mathbf{OFF}_{N_-} \end{array} \right] (\omega_k, \omega_k^2, \dots, \omega_k^{N_+}, 0, \dots, 0)^T \otimes \mathbf{z}_{\text{on}} \\ &= \left[\begin{array}{cccc|c} \mathbf{J}_{\text{on}} & \mathbf{J}_{\text{c}} & \cdots & \mathbf{J}_{\text{c}} & \\ \mathbf{J}_{\text{c}} & \mathbf{J}_{\text{on}} & \ddots & \vdots & \\ \vdots & \ddots & \ddots & \mathbf{J}_{\text{c}} & \\ \mathbf{J}_{\text{c}} & \cdots & \mathbf{J}_{\text{c}} & \mathbf{J}_{\text{on}} & \\ \hline & \mathbf{C}_{N_- \times N_+} & & & \mathbf{OFF}_{N_-} \end{array} \right] \begin{pmatrix} \omega_k \\ \omega_k^2 \\ \vdots \\ \omega_k^{N_+} \\ 0 \\ \vdots \\ 0 \end{pmatrix} \otimes \mathbf{z}_{\text{on}} \\ &= \begin{pmatrix} \mathbf{J}_{\text{on}}\omega_k & + & \sum_{j \neq 1} \omega_k^j \mathbf{J}_{\text{c}} \\ \mathbf{J}_{\text{on}}\omega_k^2 & + & \sum_{j \neq 2} \omega_k^j \mathbf{J}_{\text{c}} \\ \vdots & & \\ \mathbf{J}_{\text{on}}\omega_k^{N_+} & + & \sum_{j \neq N_+} \omega_k^j \mathbf{J}_{\text{c}} \\ \sum_{j=1}^{N_+} \omega_k^j \mathbf{J}_{\text{c}} \\ \vdots \\ \sum_{j=1}^{N_+} \omega_k^j \mathbf{J}_{\text{c}} \end{pmatrix} \otimes \mathbf{z}_{\text{on}} = \begin{pmatrix} \mathbf{J}_{\text{on}}\omega_k & - & \mathbf{J}_{\text{c}}\omega_k & + & \mathbf{J}_{\text{c}} \sum_{j=1}^{N_+} \omega_k^j \\ \mathbf{J}_{\text{on}}\omega_k^2 & - & \mathbf{J}_{\text{c}}\omega_k^2 & + & \mathbf{J}_{\text{c}} \sum_{j=1}^{N_+} \omega_k^j \\ \vdots & & & & \\ \mathbf{J}_{\text{on}}\omega_k^{N_+} & - & \mathbf{J}_{\text{c}}\omega_k^{N_+} & + & \mathbf{J}_{\text{c}} \sum_{j=1}^{N_+} \omega_k^j \\ 0 \\ \vdots \\ 0 \end{pmatrix} \otimes \mathbf{z}_{\text{on}} \\ &= \begin{pmatrix} \omega_k [\mathbf{J}_{\text{on}} - \mathbf{J}_{\text{c}}] \mathbf{z}_{\text{on}} \\ \omega_k^2 [\mathbf{J}_{\text{on}} - \mathbf{J}_{\text{c}}] \mathbf{z}_{\text{on}} \\ \vdots \\ \omega_k^{N_+} [\mathbf{J}_{\text{on}} - \mathbf{J}_{\text{c}}] \mathbf{z}_{\text{on}} \\ 0 \\ \vdots \\ 0 \end{pmatrix} = \mathbf{v}_k \otimes [\mathbf{J}_{\text{on}} - \mathbf{J}_{\text{c}}] \mathbf{z}_{\text{on}} = \mathbf{v}_k \otimes (\lambda_{\text{on}} \mathbf{z}_{\text{on}}) = \lambda_{\text{on}} (\mathbf{v}_k \otimes \mathbf{z}_{\text{on}}). \end{aligned} \tag{20}$$

The proof of $\mathbf{J}_I(\mathbf{w}_k \otimes \mathbf{z}_{\text{off}}) = \lambda_{\text{off}}(\mathbf{w}_k \otimes \mathbf{z}_{\text{off}})$ can be done analogously.

For the remaining case (19), let us consider

$$\mathbf{v} = \underbrace{(\mathbf{a}, \dots, \mathbf{a})}_{N_+}, \underbrace{(\mathbf{b}, \dots, \mathbf{b})}_{N_-}^T = \begin{pmatrix} \mathbb{1}_{N_+} \otimes \mathbf{a} \\ \mathbb{1}_{N_-} \otimes \mathbf{b} \end{pmatrix}.$$

Direct calculations lead to

$$\begin{aligned} \mathbf{J}_I \mathbf{v} &= \begin{bmatrix} \mathbf{ON}_{N_+} & \mathbf{C}_{N_+ \times N_-} \\ \mathbf{C}_{N_- \times N_+} & \mathbf{OFF}_{N_-} \end{bmatrix} \begin{pmatrix} \mathbb{1}_{N_+} \otimes \mathbf{a} \\ \mathbb{1}_{N_-} \otimes \mathbf{b} \end{pmatrix} \\ &= \begin{bmatrix} \mathbf{J}_{\text{on}} & \mathbf{J}_c & \cdots & \mathbf{J}_c & \mathbf{J}_c & \cdots & \cdots & \mathbf{J}_c \\ \mathbf{J}_c & \mathbf{J}_{\text{on}} & \ddots & \vdots & \vdots & \ddots & \ddots & \vdots \\ \vdots & \ddots & \ddots & \mathbf{J}_c & \vdots & \ddots & \ddots & \vdots \\ \mathbf{J}_c & \cdots & \mathbf{J}_c & \mathbf{J}_{\text{on}} & \mathbf{J}_c & \cdots & \cdots & \mathbf{J}_c \\ \hline \mathbf{J}_c & \cdots & \cdots & \mathbf{J}_c & \mathbf{J}_{\text{off}} & \mathbf{J}_c & \cdots & \mathbf{J}_c \\ \vdots & \ddots & \ddots & \vdots & \mathbf{J}_c & \mathbf{J}_{\text{off}} & \ddots & \vdots \\ \vdots & \ddots & \ddots & \vdots & \vdots & \ddots & \ddots & \mathbf{J}_c \\ \mathbf{J}_c & \cdots & \cdots & \mathbf{J}_c & \mathbf{J}_c & \cdots & \mathbf{J}_c & \mathbf{J}_{\text{off}} \end{bmatrix} \begin{pmatrix} \mathbf{a} \\ \vdots \\ \mathbf{a} \\ \mathbf{b} \\ \vdots \\ \mathbf{b} \end{pmatrix} \\ &= \begin{pmatrix} [\mathbf{J}_{\text{on}} + (N_+ - 1)\mathbf{J}_c]\mathbf{a} + & N_- \mathbf{J}_c \mathbf{b} \\ \vdots & \vdots \\ [\mathbf{J}_{\text{on}} + (N_+ - 1)\mathbf{J}_c]\mathbf{a} + & N_- \mathbf{J}_c \mathbf{b} \\ N_+ \mathbf{J}_c \mathbf{a} & + [\mathbf{J}_{\text{off}} + (N_- - 1)\mathbf{J}_c]\mathbf{b} \\ \vdots & \vdots \\ N_+ \mathbf{J}_c \mathbf{a} & + [\mathbf{J}_{\text{off}} + (N_- - 1)\mathbf{J}_c]\mathbf{b} \end{pmatrix} \stackrel{(19)}{=} \begin{pmatrix} \lambda \mathbf{a} \\ \vdots \\ \lambda \mathbf{a} \\ \lambda \mathbf{b} \\ \vdots \\ \lambda \mathbf{b} \end{pmatrix} = \lambda \mathbf{v}. \end{aligned}$$

Proof is complete.

Note that Lemma 1 does not deal with the cases $N_+ = 0$ and $N_+ = N$. The following lemmas treat these cases and they are given without proof, since their proof is analogous to Lemma 1.

Lemma 2 [Dimension reduction of the eigenvalue problem (case $N_+ = 0$)]. *The eigenvalue problem (16) in the case $N_+ = 0$ can be reduced to the following two eigenvalue problems*

$$[\mathbf{J}_{\text{off}} - \mathbf{J}_c]\mathbf{z} = \lambda \mathbf{z}, \quad (21)$$

$$[\mathbf{J}_{\text{off}} + (N - 1)\mathbf{J}_c]\mathbf{b} = \lambda \mathbf{b}. \quad (22)$$

More specifically, the following are the eigenvector-eigenvalue pairs of (16)

$$((\mathbf{w}_k \otimes \mathbf{z}_{\text{off}}), \lambda_{\text{off}}), \quad k = 1, \dots, N - 1$$

with

$$\mathbf{w}_k = (\mu_k, \mu_k^2, \dots, \mu_k^N)^T$$

and

$$\mu_k^j = \exp\left(\frac{2\pi i}{N} jk\right),$$

if $(\mathbf{z}_{\text{off}}, \lambda_{\text{off}})$ are the eigenvector-eigenvalue pairs of (21). Likewise,

$$(\mathbb{1}_N \otimes \mathbf{b}, \lambda)$$

is the eigenvector-eigenvalue pair of (16) if (\mathbf{b}, λ) is the eigenvector-eigenvalue pair of (22).

Lemma 3 [Dimension reduction of the eigenvalue problem (case $N_+ = N$)]. *The eigenvalue problem (16) in the case $N_+ = N$ can be reduced to the following two eigenvalue problems*

$$[\mathbf{J}_{\text{on}} - \mathbf{J}_{\text{c}}]\mathbf{z} = \lambda\mathbf{z}, \quad (23)$$

$$[\mathbf{J}_{\text{on}} + (N - 1)\mathbf{J}_{\text{c}}]\mathbf{a} = \lambda\mathbf{a}. \quad (24)$$

More specifically, the following are the eigenvector-eigenvalue pairs of (16)

$$((\mathbf{v}_k \otimes \mathbf{z}_{\text{on}}), \lambda_{\text{on}}), \quad k = 1, \dots, N - 1$$

with

$$\mathbf{v}_k = (\omega_k, \omega_k^2, \dots, \omega_k^N)^T$$

and

$$\omega_k^j = \exp\left(\frac{2\pi i}{N}jk\right),$$

if $(\mathbf{z}_{\text{on}}, \lambda_{\text{on}})$ are the eigenvector-eigenvalue pairs of (23). Likewise,

$$(\mathbb{1}_N \otimes \mathbf{a}, \lambda)$$

is the eigenvector-eigenvalue pair of (16) if (\mathbf{a}, λ) is the eigenvector-eigenvalue pair of (24). After reducing the original problem (16) for the stability of the critical manifold into low-dimensional problems in Lemmas 1-3, we present the eigenvalues of these reduced problems in lemma 4.

Lemma 4 [Eigenvalues].

1) *The solutions of the eigenvalue problem*

$$[\mathbf{J}_{\text{on}} - \mathbf{J}_{\text{c}}]\mathbf{z} = \lambda\mathbf{z}$$

are given by the solutions of

$$\lambda^2 + \gamma(x_I + 1)\lambda + x_I\gamma = 0, \quad \text{where } x_I := \delta - 1 + k[\omega + f(X_I)].$$

2) *The solutions of the eigenvalue problem*

$$[\mathbf{J}_{\text{off}} - \mathbf{J}_{\text{c}}]\mathbf{z} = \lambda\mathbf{z}$$

are $\lambda_1 = -\gamma$ and $\lambda_2 = x_I$.

3) *The solutions of the eigenvalue problem*

$$[\mathbf{J}_{\text{on}} + (N - 1)\mathbf{J}_{\text{c}}]\mathbf{a} = \lambda\mathbf{a}$$

are given as solutions of

$$\lambda^2 + \gamma(x_I + 1)\lambda - x_I\gamma(\xi_I - 1) = 0, \quad \text{where } \xi_I := \frac{kA\alpha}{1 + \alpha X_I}.$$

4) *The eigenvalue problem*

$$[\mathbf{J}_{\text{off}} + (N - 1)\mathbf{J}_{\text{c}}]\mathbf{b} = \lambda\mathbf{b}$$

has the same eigenvalues as 2), i.e. $\lambda_1 = -\gamma$ and $\lambda_2 = x_I$.

5) *The eigenvalue problem*

$$\begin{bmatrix} [\mathbf{J}_{\text{on}} + (N_+ - 1)\mathbf{J}_{\text{c}}] & N_- \mathbf{J}_{\text{c}} \\ N_+ \mathbf{J}_{\text{c}} & [\mathbf{J}_{\text{off}} + (N_- - 1)\mathbf{J}_{\text{c}}] \end{bmatrix} \begin{pmatrix} \mathbf{a} \\ \mathbf{b} \end{pmatrix} = \lambda \begin{pmatrix} \mathbf{a} \\ \mathbf{b} \end{pmatrix}$$

has the eigenvalues $\lambda_1 = -\gamma$ and $\lambda_2 = x_I$ and, additionally, the solutions of

$$\lambda^2 + \gamma(x_I + 1)\lambda - x_I\gamma \left(\frac{N_+}{N} \xi_I - 1 \right) = 0.$$

Proof. We will only give direct calculations of the characteristic polynomial for cases 3–5, as cases 1 and 2 are even more straightforward.

3) Let us define

$$\mathbf{A} := \mathbf{J}_{\text{on}} + (N - 1)\mathbf{J}_{\text{c}},$$

$$\xi_I := \frac{kA\alpha}{1 + \alpha X_I}, \quad \text{and } x_I := \delta - 1 + k(\omega + f(X_I)).$$

Then we obtain the characteristic polynomial $\chi_{\mathbf{A}}(\lambda)$ as follows:

$$\begin{aligned} \chi_{\mathbf{A}}(\lambda) &= \det(\mathbf{A} - \lambda\mathbf{I}) \\ &= \det(\mathbf{J}_{\text{on}} + (N - 1)\mathbf{J}_{\text{c}} - \lambda\mathbf{I}) \\ &= \det \left(\begin{pmatrix} 0 & x_I \\ \gamma(N^{-1}\xi_I - 1) & -\gamma(x_I + 1) \end{pmatrix} + \begin{pmatrix} 0 & 0 \\ (N - 1)\gamma N^{-1}\xi_I & 0 \end{pmatrix} - \begin{pmatrix} \lambda & 0 \\ 0 & \lambda \end{pmatrix} \right) \\ &= \det \begin{pmatrix} -\lambda & x_I \\ \gamma(\xi_I - 1) & -\gamma(x_I + 1) - \lambda \end{pmatrix} \end{aligned}$$

$$= \lambda^2 + \gamma(x_I + 1)\lambda - x_I\gamma(\xi_I - 1).$$

4) Let us define

$$\mathbf{B} := \mathbf{J}_{\text{off}} + (N - 1)\mathbf{J}_c,$$

and let ξ_I, x_I be as in the calculations of $\chi_{\mathbf{A}}(\lambda)$. Then we obtain the characteristic polynomial $\chi_{\mathbf{B}}(\lambda)$ as follows:

$$\begin{aligned} \chi_{\mathbf{B}}(\lambda) &= \det(\mathbf{B} - \lambda\mathbf{I}) \\ &= \det(\mathbf{J}_{\text{off}} + (N - 1)\mathbf{J}_c - \lambda\mathbf{I}) \\ &= \det\left(\begin{pmatrix} x_I & 0 \\ \gamma(N^{-1}\xi_I - x_I - 1) & -\gamma \end{pmatrix} + \begin{pmatrix} 0 & 0 \\ (N - 1)\gamma N^{-1}\xi_I & 0 \end{pmatrix} - \begin{pmatrix} \lambda & 0 \\ 0 & \lambda \end{pmatrix}\right) \\ &= \det\begin{pmatrix} x_I - \lambda & 0 \\ \gamma(\xi_I - x_I - 1) & -\gamma - \lambda \end{pmatrix} \\ &= (\lambda - x_I)(\lambda - (-\gamma)). \end{aligned}$$

5) Again, let ξ, x_I be as in the calculations of $\chi_{\mathbf{A}}(\lambda)$. Then the characteristic equation for the case 5) is

$$\begin{aligned} &\det\begin{pmatrix} -\lambda & x_I & 0 & 0 \\ \gamma(N_+N^{-1}\xi_I - 1) & -\gamma(x_I + 1) - \lambda & \gamma N_-N^{-1}\xi_I & 0 \\ 0 & 0 & x_I - \lambda & 0 \\ \gamma N_+N^{-1}\xi_I & 0 & \gamma(N_-N^{-1}\xi_I - x_I - 1) & -\gamma - \lambda \end{pmatrix} \\ &= (-\gamma - \lambda) \det\begin{pmatrix} -\lambda & x_I & 0 \\ \gamma(N_+N^{-1}\xi_I - 1) & -\gamma(x_I + 1) - \lambda & \gamma N_-N^{-1}\xi_I \\ 0 & 0 & x_I - \lambda \end{pmatrix} \\ &= (-\gamma - \lambda)(x_I - \lambda) \det\begin{pmatrix} -\lambda & x_I \\ \gamma(N_+N^{-1}\xi_I - 1) & -\gamma(x_I + 1) - \lambda \end{pmatrix} \\ &= (\lambda - (-\gamma))(\lambda - x_I) \left(\lambda^2 + \gamma(x_I + 1)\lambda - x_I\gamma \left(\frac{N_+}{N} \xi_I - 1 \right) \right). \end{aligned}$$

Proof is finished.

Using the obtained results in Lemma 1 and Lemma 4, we can obtain explicit stability conditions for the critical manifolds.

Lemma 5. [Stability of the critical manifolds in symmetric case] *Consider the symmetric case with $\delta_1 = \dots = \delta_N$. Then the "off" branch B_0 of the critical manifold is exponentially stable if and only if*

$$\omega < \frac{1 - \delta}{k}. \quad (25)$$

The "all on" branch B_1 is exponentially stable if and only if

$$X_1 > kA - \frac{1}{\alpha}.$$

All other branches are unstable for all parameter values.

Proof. We consider different cases:

1) $N_+ = 0$: According to Lemmas 2 and 4, the eigenvalues in this case are $\lambda_1 = -\gamma$ and $\lambda_2 = x_I$. Since $\gamma > 0$, consequently $\lambda_1 < 0$ always holds true. From $\lambda_2 < 0$, we obtain the first criterion for the exponential stability

$$x_I = \delta + k(\omega + f(X_I)) - 1 = \delta + k\omega - 1 < 0,$$

which is equivalent to (25).

2) $1 \leq N_+ < N$: According to Lemmas 1 and 4, the eigenvalues in this case are given by

$$\lambda^2 + \gamma(x_I + 1)\lambda + x_I\gamma = 0,$$

$$\lambda^2 + \gamma(x_I + 1)\lambda - x_I\gamma\left(\frac{N_+}{N}\xi_I - 1\right) = 0, \quad (26)$$

as well as $\lambda_1 = -\gamma$ and $\lambda_2 = x_I$. Since

$$x_I = \frac{N}{N_+}X_+, \quad (27)$$

we have $\lambda_2 > 0$ and these branches are always unstable.

3) $N_+ = N$: In this case the eigenvalues are given by

$$\lambda^2 + \gamma(x_I + 1)\lambda + x_I\gamma = 0 \quad (28)$$

and

$$\lambda^2 + \gamma(x_I + 1)\lambda - x_I\gamma(\xi_I - 1) = 0. \quad (29)$$

For the polynomial (28), we see that its coefficients are positive, hence it can have only negative solutions. For the polynomial (29), we obtain the following stability criterion

$$-x_I\gamma(\xi_I - 1) > 0,$$

which leads to

$$X_I > \frac{kA\alpha - 1}{\alpha} = kA - \frac{1}{\alpha}.$$

Proof is complete.

A.II. CRITICAL MANIFOLD IN THE SYMMETRIC CASE

Figure 5 shows the structure of the critical manifolds for the case of three identical lasers with $\delta_1 = \delta_2 = \delta_3$. This resembles Figs. 3(a,b) in the main manuscript, which depict the non-symmetric scenario. Stability details for Fig. 5 are provided in Lemma 5. The figure demonstrates that the CC phenomenon is absent in the symmetric scenario, while also helping to identify the alterations in the critical manifold's configuration due to the lasers' heterogeneity. In particular, it can be observed that all branches corresponding to the same number of lasers 'on' are projected onto the same line and have the same stability. Furthermore, all branches branch out from a single point S.

A.III. HETEROCLINIC CONNECTIONS BETWEEN BRANCHES OF THE CRITICAL MANIFOLD

A.III.1 Existence of heteroclinic connections

Heteroclinic connections (orbits) for a fixed value of the slow variable ω are the orbits of the fast subsystem $(\mathbf{x}(t), \mathbf{y}(t))$ connecting its different equilibria. Since these equilibria are on different branches of the critical manifolds B_I and B_J , the heteroclinic orbits create connections between the branches. More precisely, we have

$$(\mathbf{x}(t), \mathbf{y}(t)) \rightarrow B_J \text{ as } t \rightarrow +\infty \quad \text{and} \quad (\mathbf{x}(t), \mathbf{y}(t)) \rightarrow B_I \text{ as } t \rightarrow -\infty.$$

for a fixed ω and $\varepsilon = 0$ in Eq. (2) of the main manuscript.

For small but non-zero ε , the critical manifolds persist as perturbed slow manifolds, and the heteroclinic connections persist between the branches of the slow manifolds (see the robustness discussion in sec. A.III.2). As a result, a one-parameter family of connecting orbits appears, connecting B_I to B_J , parameterised by ω .

The way to represent the heteroclinic connections for a fixed ω is to treat the equilibria of the fast subsystem as nodes and the heteroclinic connections as directed links of some network. The result is a directed network of heteroclinic connections. Obviously, the equilibria, i.e. the nodes, can be equivalently denoted by the corresponding branches B_I of the critical manifold. The result is a network like the one shown in Fig. 3(c) of the main manuscript.

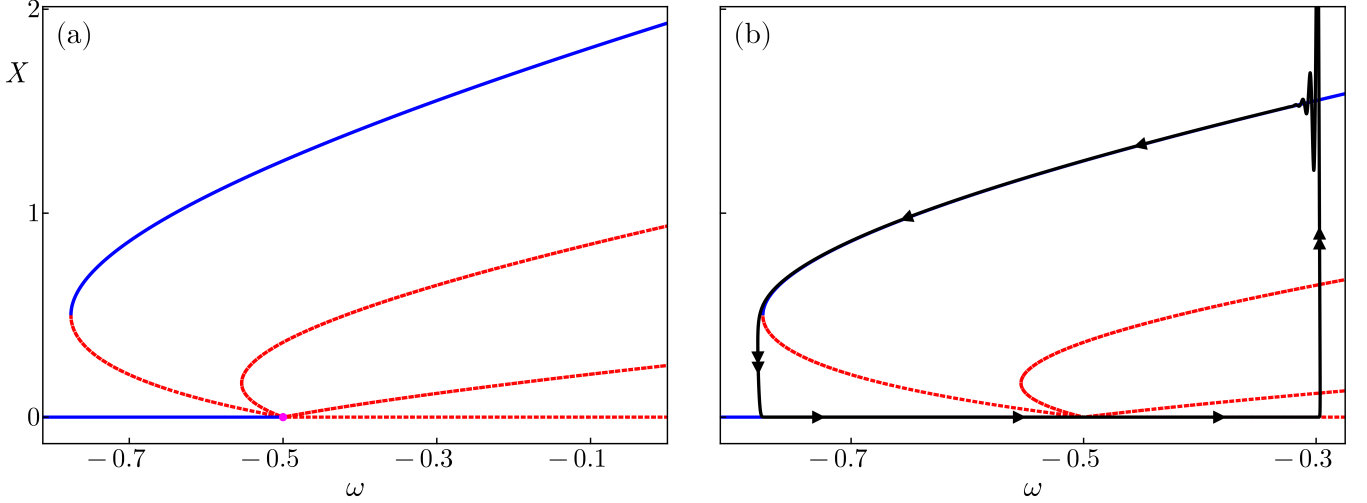


FIG. 5. Critical manifolds for the symmetric case. The colors and line styles have the same meaning as in Figs. 3(a,b) of the main manuscript. In addition, the one branching point S is shown in magenta. Parameters: $\delta_1 = \delta_2 = \delta_3 = 1.35$, $k = 0.7$, $A = k^{-1}$, and $\alpha = 2$.

Figure 6 shows how the network of heteroclinic connections changes with ω . Here, we do not present a rigorous proof, but rather simple numerical simulations: starting from an unstable equilibrium, we added a small perturbation of size 10^{-6} in the direction of its unstable eigenvectors and obtained the corresponding trajectories from the simulation. The heteroclinic trajectory is recorded when the solution arrives in a 10^{-6} neighbourhood of another equilibrium. Note that another argument for the existence of heteroclinic connections is that, due to the general properties of local transcritical bifurcation, there exists a connection close to the branching point [1]. As a result, the heteroclinic network evolves with ω so that it has the form as in Fig. 3(c) of the main manuscript for $\omega > \frac{1-\delta_1}{k}$.

A.III.2 Robustness of heteroclinic connections

In the following we use the following conclusion of the transversality theorem from differential topology [2]: If two submanifolds X and Z of \mathbb{R}^n are transversal, then their intersection $X \cap Z$ is a submanifold of \mathbb{R}^n and

$$\text{codim}(X \cap Z) = \text{codim } X + \text{codim } Z.$$

In terms of dimensions, in our case this means

$$\dim(X \cap Z) = (\dim X + \dim Z) - n.$$

We will show the following for the heteroclinic connection $p \rightarrow q$:

$$\dim(W_{\text{loc}}^u(p)) + \dim(W_{\text{loc}}^s(q)) > n, \quad (30)$$

where W_{loc}^u is the unstable manifold of equilibrium p and $W_{\text{loc}}^s(q)$ is the stable manifold of equilibrium q . This will imply that if $W_{\text{loc}}^u(p)$ and $W_{\text{loc}}^s(q)$ intersect transversely, the intersection is a submanifold of dimension ≥ 1 , i.e. there is at least one heteroclinic connection, and this intersection is robust [2]. We will not give the proof of the transversality here, which remains a missing ingredient for a rigorous proof of heteroclinic connections. Since such a rigorous proof is not our main purpose, we leave it as an open problem.

Lemma 6 [Dimensionality of W_{loc}^u]. *The dimension of the local unstable manifold W_{loc}^u at the equilibrium of the fast subsystem in the symmetric case is given for $\omega \geq \frac{1-\delta}{k}$ by*

1) $N_+ = 0$:

$$\dim(W_{\text{loc}}^u) = N$$

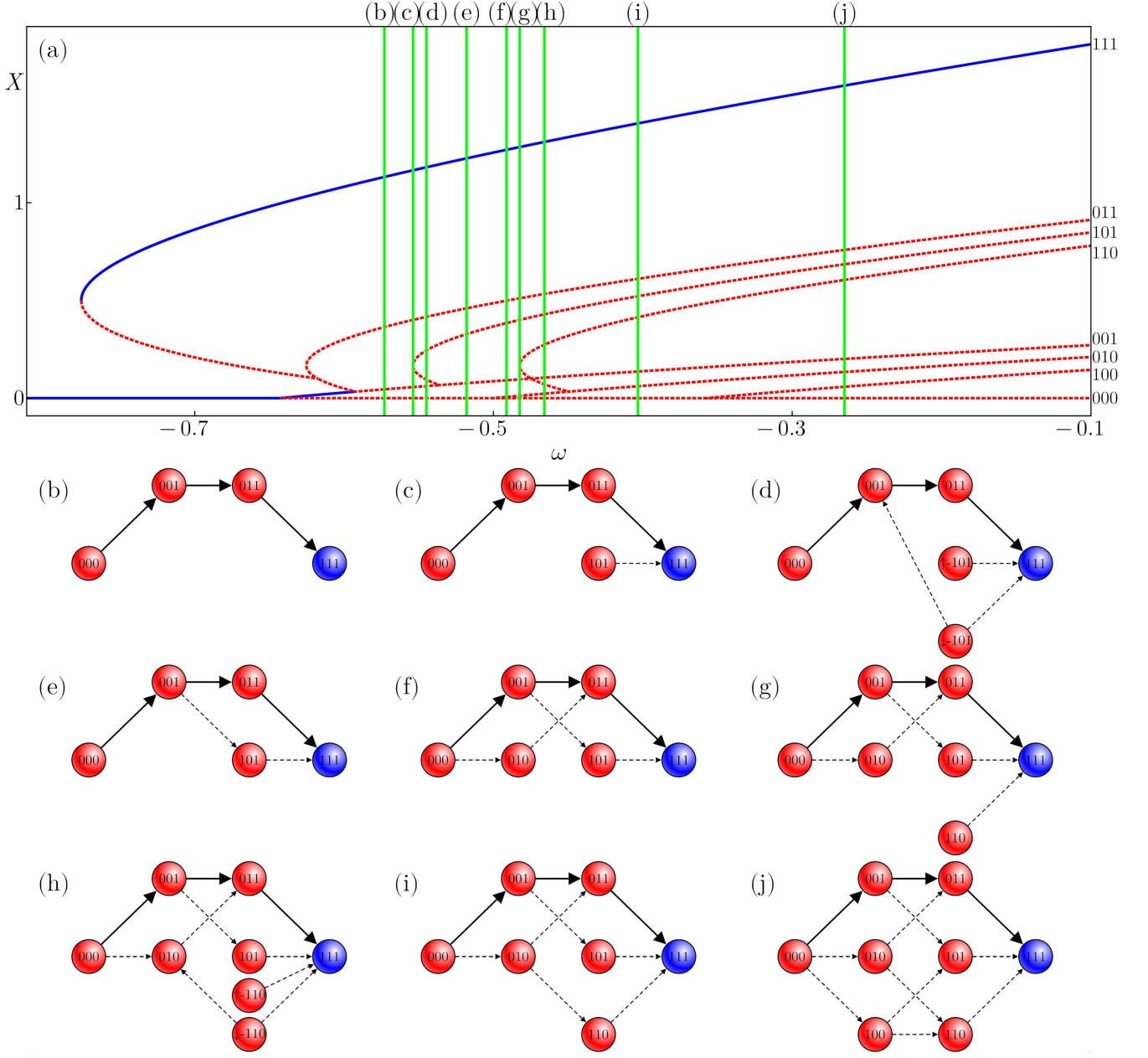


FIG. 6. Transitions of the heteroclinic connections graph of the non-symmetric case starting at ω_b where ω_b is the ω -value of the second branching point along the 001 branch where 001 branch becomes unstable (see (a)). (b) graph before the 101 fold point. (c) graph at the 101 fold point. (d) graph after the 101 fold point before the 101 branching point. (e) graph after the 101 branching point before the second 000 branching point. (f) graph after the second 000 branching point before the 110 fold point. (g) graph at the 110 fold point. (h) graph after the 110 fold point before the 110 branching point. (i) graph after the 110 branching point before the third 000 branching point. (j) graph after the third 000 branching point.

2) $N_+ > 0$:

$$\dim(W_{\text{loc}}^u) = \begin{cases} N_-, & \text{for } X_I > \frac{N_+}{N} kA - \alpha^{-1} \\ N_- + 1, & \text{for } X_I \leq \frac{N_+}{N} kA - \alpha^{-1}. \end{cases}$$

Proof. In the case of $N_+ = 0$, we obtain from both reduced eigenvalue problems (22), (21) the eigenvalues $\lambda_1 = -\gamma$ and $\lambda_2 = x_I$ of which only λ_2 is unstable for $\omega \geq \frac{1-\delta}{k}$. Clearly, since there are two distinct eigenvalues for each of the reduced system of size 2, each eigenvalue has a geometric multiplicity of one. Say these eigenvectors of λ_2 are \mathbf{b}_2 and

\mathbf{z}_2 of the reduced eigenvalue problems (22), (21) respectively, then the eigenvectors of the original eigenvalue problem are $(\mathbf{w}_0 \otimes \mathbf{b}_2), (\mathbf{w}_1 \otimes \mathbf{z}_2), \dots, (\mathbf{w}_{N_- - 1} \otimes \mathbf{z}_2)$. Therefore,

$$\dim(W_{\text{loc}}^u) = N_- = N.$$

For the remaining case $0 < N_+ \leq N$, we use the following property of the solutions λ_3 and λ_4 of the polynomial (26):

- $\lambda_3 < 0$ and $\lambda_4 < 0$ for $X_I > \frac{N_+}{N}kA - \frac{1}{\alpha}$;
- $\lambda_3 > 0$ and $\lambda_4 < 0$ for $X_I \leq \frac{N_+}{N}kA - \frac{1}{\alpha}$.

Let \mathbf{a}_3 be the eigenvector of λ_3 . Then we have

Case $0 < N_+ < N$ and $X_I \leq \frac{N_+}{N}kA - \frac{1}{\alpha}$:

$$\dim(W_{\text{loc}}^u) = \dim(\{(\mathbf{v}_0 \otimes \mathbf{a}_3), (\mathbf{w}_0 \otimes \mathbf{b}_2), (\mathbf{w}_1 \otimes \mathbf{z}_2), \dots, (\mathbf{w}_{N_- - 1} \otimes \mathbf{z}_2)\}) = N_- + 1$$

Case $0 < N_+ < N$ and $X_I > \frac{N_+}{N}kA - \frac{1}{\alpha}$:

$$\dim(W_{\text{loc}}^u) = \dim(\{(\mathbf{w}_0 \otimes \mathbf{b}_2), (\mathbf{w}_1 \otimes \mathbf{z}_2), \dots, (\mathbf{w}_{N_- - 1} \otimes \mathbf{z}_2)\}) = N_-$$

Case $N_+ = N$ and $X_I \leq \frac{N_+}{N}kA - \frac{1}{\alpha}$:

$$\dim(W_{\text{loc}}^u) = \dim(\{(\mathbf{v}_0 \otimes \mathbf{a}_3)\}) = 1 = N_- + 1$$

Case $N_+ = N$ and $X_I > \frac{N_+}{N}kA - \frac{1}{\alpha}$:

$$\dim(W_{\text{loc}}^u) = 0$$

where, besides the result for $N_+ = 0$, we additionally used that \mathbf{v}_0 and $\{\mathbf{w}_m\}_{m=0, \dots, N_- - 1}$ are linearly independent. *Proof is complete.*

Lemma 6 immediately implies that $\dim(W_{\text{loc}}^u(B_{000})) + \dim(W_{\text{loc}}^s(B_J)) = 2N + 1$, where J is one of the branches with a single laser on, provided the parameter ω is sufficiently large (beyond the branching points). The same holds for the transition between neighboring branches where N_- changes by one, provided $X_I > \frac{N_+}{N}kA - \alpha^{-1}$, which means that the branch is considered beyond the fold point.

The results of Lemma 6 are illustrated in Fig. 7(a) for the case of three lasers. From the results for the symmetric case, the asymmetric case with weakly inhomogeneous δ_i can be deduced using continuation arguments and the fact that hyperbolic equilibria are robust to small parameter changes, see Fig. 7(b). This means that Lemma 6 can be applied to a weakly non-symmetric case.

Figure 8 illustrates the graphs of possible heteroclinic connections with the edges annotated by the minimal value of the sum of the dimensions $\dim(W_{\text{loc}}^u(B_I)) + \dim(W_{\text{loc}}^s(B_J))$. Before proceeding, for the non-symmetric case, we need to further specify what is meant by "graph of possible heteroclinic connections". For this, one can convince oneself by comparing Figs. 6(b), (c), (e), (f), (g), (i), (j) and Fig. 8(b) that the graphs for different values of ω (not considering fold and branching points) are subgraphs of Fig. 8. For the symmetric case there is no need for these considerations as the graph of possible connections and the actual graph of connections coincide. Consequently Figure 8(a) shows the case that is given by Lemma 6 for the symmetric system beyond the branching point $\omega > \omega_b = \frac{1-\delta}{k}$. Note that in the asymmetric case in Fig. 8(b) the condition (30) is not fulfilled, but the heteroclinic connections do exist due to the existence of invariant subspaces. Within these invariant subspaces, the corresponding heteroclinic orbit connects a saddle with one unstable direction to an attractor. For example, the connection $B_{000} \rightarrow B_{001}$ is realized within a 4-dimensional invariant subspace defined by $x_1 = x_2 = 0$. Hence, the condition (30) holds for $N = 4$.

A.IV. JUMP POINTS

Let us first consider the jump from the branch B_{000} in the case of three lasers. The motion during this jump is illustrated in Fig. 4 of the main manuscript, see the part AC:

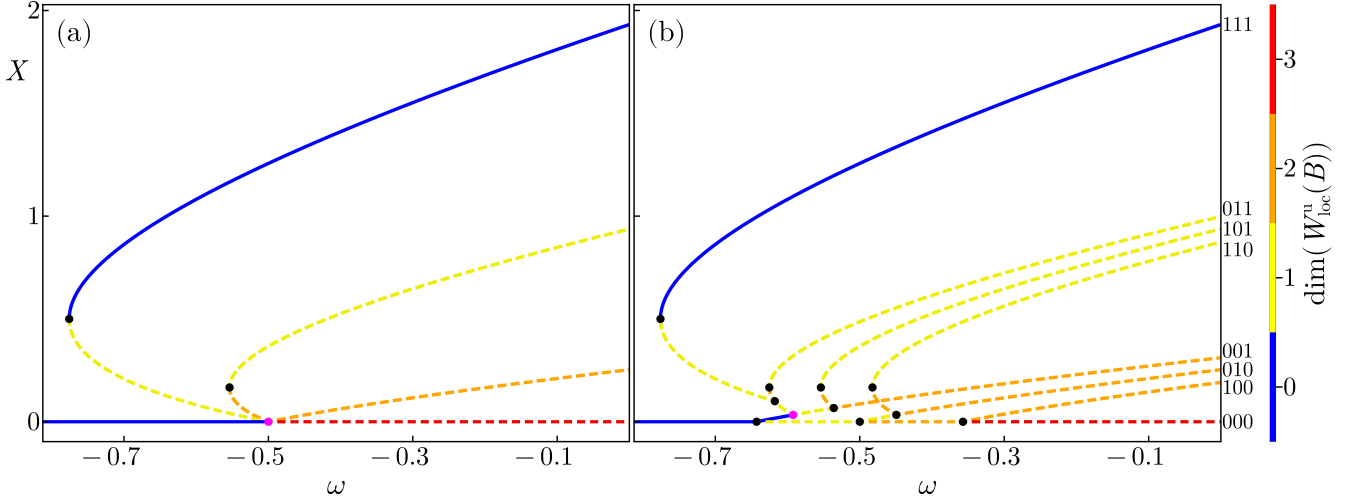


FIG. 7. Dimensions of unstable manifolds $\dim(W_{\text{loc}}^u)$ along the branches of the critical manifold. The dimensions correspond to the number of unstable eigenvalues of the fast subsystem for fixed ω ; their number changes at the transcritical and fold points (black dots). The transcritical points which define the beginning of the examined interval of heteroclinic connections $\omega \in (\omega_b, 0]$ are shown in magenta (see Fig. 8). Parameter values are the same as in Fig. 5 for (a) and as in Fig. 3 of the main manuscript.

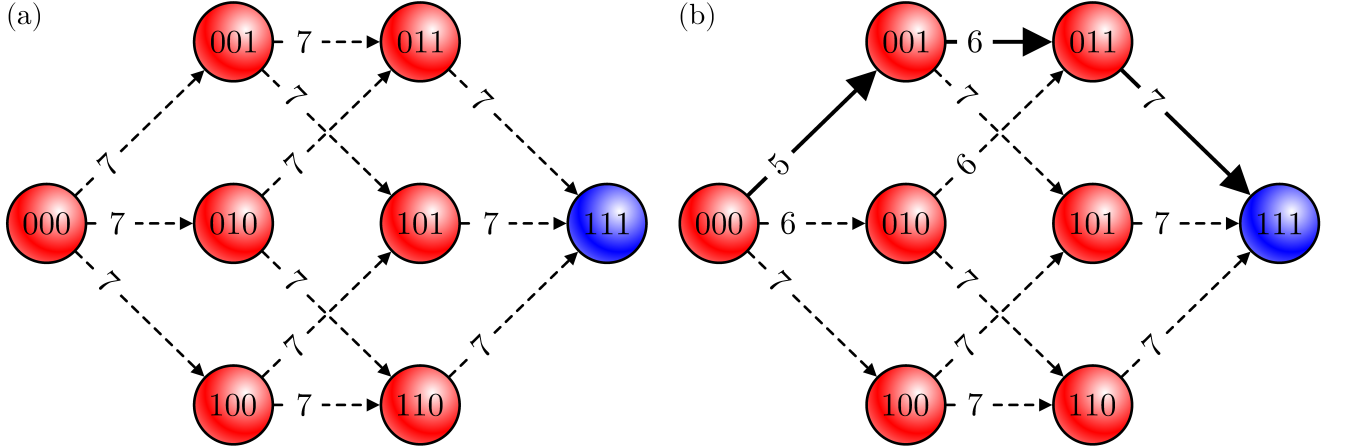


FIG. 8. Graph of possible heteroclinic connections. Edges are annotated by the minimal value of the sum $\dim(W_{\text{loc}}^u(B_I)) + \dim(W_{\text{loc}}^s(B_J))$ for the existing connections $B_I \rightarrow B_J$, see eq. (30) for $\omega \in (\omega_b, 0]$, where $\omega_b = \frac{1-\delta}{k}$ and all δ_i are the same for the symmetric case, $\omega_b = \frac{1-\delta_2}{k} - A \ln(1 + \alpha X_{001})$ for the nonsymmetric case.

- The part AB: convergence to the branch B_{000} with the rate corresponding to the maximal (least stable) eigenvalue of the corresponding equilibrium of the fast subsystem; we call it $\mu_1^{000}(\omega)$, where we have explicitly written the dependence of this eigenvalue on ω .
- BC: repulsion from the branch B_{000} . We assume that there the eigenvalues do not change their order, and this repulsion takes place with the same rate $\mu_1^{000}(\omega)$, where $\mu_1^{000}(\omega)$ changes its sign to positive at ω_B in point B.

Thus, the small Δ distance to the B_{000} branch can be approximated by the linearized dynamics within the leading manifold $W^l(B_{000})$

$$\frac{d\Delta}{dt} \simeq \mu_1^{000}(\omega(t))\Delta(t). \quad (31)$$

As a side note, we have used here that the branch B_{000} does not change with ω . The latter equation can be rewritten with respect to ω instead of time:

$$\begin{aligned} \frac{d\Delta}{dt} &= \frac{d\Delta}{d\omega} \frac{d\omega}{dt} = \frac{d\Delta}{d\omega} [-\varepsilon(\omega + f(X_{000}))], \\ \Rightarrow \frac{d\Delta}{d\omega} &= -\frac{1}{\varepsilon(\omega + f(X_{000}))} \mu_1^{000}(\omega) \Delta(\omega), \end{aligned} \quad (32)$$

and the subsequent solution of the differential equation in (32) gives

$$\Delta(\omega_C) = \Delta(\omega_A) \exp \left[-\frac{1}{\varepsilon} \int_{\omega_A}^{\omega_C} \frac{\mu_1^{000}(\omega)}{\omega + f(X_{000})} d\omega \right],$$

where ω_A is the drop point, i.e. the point where the dynamics return to the B_{000} branch, X_{000} is the mean field at the branch B_{000} , and ω_C denotes the ω -value of the first jump. Then we assume that the jump point is given

$$\Delta(\omega_C) \approx \Delta(\omega_A),$$

resulting in the final jump point condition

$$\int_{\omega_A}^{\omega_C} \frac{\mu_1^{000}(\omega)}{\omega + f(X_{000})} d\omega = 0. \quad (33)$$

Following similar reasoning, the second jump from the branch B_{001} to B_{011} (see point E in Fig. 4 of the main manuscript) is described by the whole trajectory part AE:

- AB: Convergence to the leading manifold $W^l(B_{000})$ corresponding to the second least stable direction along B_{000} . This convergence is governed by the second largest eigenvalue of the corresponding equilibrium of the fast subsystem; we call it $\mu_2^{000}(\omega)$.
- BC: In part BC, the leading manifold is still exponentially stable with the convergence rate given by $\mu_2^{000}(\omega)$.
- CD: At point C, the orbit jumps to the vicinity of the branch B_{001} . This happens on the fast timescale, so the contribution to the distance to $W^l(B_{000})$ is negligible.
- DE: Starting from the point D, the repulsion from the branch B_{001} (and from $W^l(B_{000})$) takes place at the exponential rate governed by the most unstable eigenvalue μ_1^{001} of the branch B_{001} .

Summing up the convergence and repulsion processes described above, we obtain the following condition for the coordinate ω_E of the jump point E:

$$\int_{\omega_A}^{\omega_C} \frac{\mu_2^{000}(\omega)}{\omega + f(X_{000})} d\omega + \int_{\omega_C}^{\omega_E} \frac{\mu_1^{001}(\omega)}{\omega + f(X_{001})} d\omega = 0. \quad (34)$$

Note that we have neglected the ω dependence of the B_{001} branch, which will probably lead to an error even if $\varepsilon \rightarrow 0$. However, the numerical test in Fig. 3 shows that (34) is already a decent approximation, and we decided not to go into more quantitative details, since the qualitative picture is clear.

Using similar arguments, we obtain an approximation for the third jump point:

$$\int_{\omega_A}^{\omega_C} \frac{\mu_3^{000}(\omega)}{\omega + f(X_{000})} d\omega + \int_{\omega_C}^{\omega_E} \frac{\mu_2^{001}(\omega)}{\omega + f(X_{001})} d\omega + \int_{\omega_E}^{\omega_G} \frac{\mu_1^{011}(\omega)}{\omega + f(X_{011})} d\omega = 0.$$

Numerical results for our example using the obtained approximations (33), (34), (35) are shown in Fig. 3 of the main manuscript.

[1] Y. Kuznetsov, *Elements of Applied Bifurcation Theory*, Vol. 112 (Springer-Verlag, 1995) p. 591.
[2] V. Guillemin and A. Pollack, *Differential Topology* (Prentice-Hall, Englewood Cliffs, N.J, 1974).